Research Article | Vol. 30, No. 23 / 7 Nov 2022 / Optics Express 42762
Optics EXPRESS

Spectroscopy and 2.1 µm laser operation of Czochralski-grown Tm^{3+}:$YScO_3$ crystals

ANNA SUZUKI,[1,2,3,*] SASCHA KALUSNIAK,[1] HIROKI TANAKA,[1] MARIO BRÜTZAM,[1] STEFFEN GANSCHOW,[1] MASAKI TOKURAKAWA,[2,3] AND CHRISTIAN KRÄNKEL[1]

[1]*Leibniz-Institut für Kristallzüchtung (IKZ), Max-Born-Str. 2, 12489 Berlin, Germany*
[2]*Institute for Laser Science, University of Electro-Communications, 1-5-1 Chofugaoka, Chofu, Tokyo 182-8585, Japan*
[3]*Center for Neuroscience and Biomedical Engineering, University of Electro-Communications, 1-5-1, Chofugaoka, Chofu, 182-8585, Japan*
[*]*a_suzuki@ils.uec.ac.jp*

Abstract: We report on growth, temperature-dependent spectroscopy, and laser experiments of Tm^{3+}-doped $YScO_3$ mixed sesquioxide crystals. For the first time, cm^3-scale laser quality Tm^{3+}:$YScO_3$ crystals with 2.2 at.% and 3.1 at.% doping levels were grown by the Czochralski method from iridium crucibles. We reveal that the structural disorder in the mixed crystals allows for broad and smooth spectral features even at cryogenic temperatures. We obtained the first continuous wave laser operation in this material at wavelengths around 2100 nm using a laser diode emitting at 780 nm as a pump source. A maximum slope efficiency of 45% was achieved using a Tm^{3+} (3.1 at.%):$YScO_3$ crystal. Our findings demonstrate the high potential of Tm^{3+}-doped mixed sesquioxides for efficient ultrafast pulse generation in the 2.1 µm range.

1. Introduction

Tm^{3+}-doped materials are attractive for highly efficient 2 µm lasers and amplifiers with high output power levels [1,2]. Tm^{3+} ions exhibit their absorption band around 790 nm corresponding to the transition from the $^3H_6$ ground state multiplet into the $^3H_4$ multiplet. This transition is suitable for pumping by commercially available high-power AlGaAs laser diodes (LDs). At sufficiently high doping concentrations, the ground state absorption of Tm^{3+}-ions is followed by a cross-relaxation process $^3H_4 \rightarrow {}^3F_4/{}^3H_6 \rightarrow {}^3F_4$, resulting in two excited Tm^{3+} ions into the upper laser level $^3F_4$ by only one pump photon. This "two-for-one" pumping scheme enables quantum efficiencies close to 2 in materials where the cross-relaxation is highly resonant. In this way, slope efficiencies up to ~80% were realized despite the low Stokes efficiency of only ~40% [3].

Tm^{3+}-doped cubic sesquioxides (Tm^{3+}:RE_2O_3, RE = Lu, Y, or Sc) are excellent gain media due to their superior spectroscopic and thermo-mechanical properties. Owing to their strong crystal field, the emission band of the laser transition $^3F_4 \rightarrow {}^3H_6$ extends to wavelengths exceeding 2100 nm, which is among the longest lasing wavelengths on this transition in Tm^{3+}-doped materials [4]. The absence of reabsorption and water vapor absorption at such long wavelengths enables broad effective gain bandwidths. This is desirable for ultrashort pulse generation. Besides, sesquioxide materials exhibit high thermal conductivities [5] and comparably weak thermal expansion [6], which facilitates efficient high-power laser operation. Nearly 50 W of output power at 59% slope efficiency were demonstrated with Tm:Lu_2O_3 [4]. Therefore, sesquioxides are excellent host materials for highly efficient, high-power continuous wave (cw) lasers [7–10] as well as ultrashort pulse lasers [11–13].

The growth of the cubic rare-earth sesquioxides is challenging due to their extremely high melting points exceeding 2350°C. The most established growth techniques to obtain high-quality cm^3-scale laser crystals are crucible-based. However, iridium, which is the most common crucible

#475711 https://doi.org/10.1364/OE.475711
Journal © 2022 Received 19 Sep 2022; revised 19 Oct 2022; accepted 27 Oct 2022; published 4 Nov 2022

Optics EXPRESS

material for the growth of oxide crystals, is not suitable for such high temperatures. Rhenium is the only available crucible material in this case. It sustains the high growth temperatures and is chemically inert to melt at the required growth atmospheres. In fact, laser-quality cm^3-scale sesquioxide crystals were successfully grown by the heat exchanger method (HEM) from rhenium crucibles [14]. However, rhenium crucibles are difficult to fabricate and thus quite expensive. Moreover, these are sensitive to oxygen in the growth atmosphere, which imposes significant difficulties during the growth of high quality sesquioxide crystals.

In recent years, also sesquioxide laser ceramics gained attention. These can be fabricated at sintering temperatures of only ~1700°C, which is considerably below their melting point. In addition, the ceramics technology is especially suitable for materials with a cubic crystal structure such as sesquioxides. There are several successful reports on the fabrication of Tm^{3+}-doped sesquioxide ceramics [15–19] as well as cw [20–22] and mode-locked lasers based on these [23,24]. However, the fabrication of high quality sesquioxide ceramics is challenging, and their laser efficiency does not reach the results obtained with single crystalline sesquioxides [25], which can be partly attributed to a tendency for increased scattering at grain boundaries, pores, and secondary phases introduced by sintering aids such as ZrO_2 or LiF [26,27].

Very recently, the phase diagram of mixed sesquioxide crystals was re-investigated [28], and mixed sesquioxide crystal compositions with melting temperatures below 2150°C were identified. This temperature range is suitable for the conventional Czochralski method using iridium crucibles to grow large-size high-quality laser crystals. Up to now, mixed sesquioxide crystals doped with Er^{3+} and Yb^{3+} have been successfully grown by the Czochralski method. and using Yb^{3+}:$YScO_3$, highly efficient laser operation was demonstrated [29]. Furthermore, mixed materials exhibit continuously broadened spectra due to inhomogeneous spectral broadening caused by their disordered structure. This is attributed to a random distribution of Y^{3+} and Sc^{3+} on the two cation sites in the cubic $Ia\bar{3}$ structure. The resulting broad and flat emission spectra are ideal for short pulse generation by mode-locking technique [30,31]. Moreover, the broadened absorption lines are useful for efficient diode pumping since LDs usually exhibit relatively broad emission spectral bandwidths, and their operating wavelength varies with temperature and operation current.

In this study, we report on the Czochralski growth and optical spectroscopy of Tm^{3+}:$YScO_3$ crystals and demonstrate the first diode-pumped laser operation in this material. Temperature-dependent absorption and emission spectra and fluorescence lifetimes were measured to reveal the potential for laser operation. Under pumping with a 780 nm LD, we obtained slope efficiencies of up to 45% at a wavelength of 2.1 µm using a Tm(3.1 at.%):$YScO_3$ crystal.

2. Crystal growth

Tm^{3+}:$YScO_3$ crystals were grown by the Czochralski method from an iridium crucible. The raw materials of Tm_2O_3, Y_2O_3, and Sc_2O_3 powders with a purity of 99.999% (5N) were prepared according to the composition $(Tm_{0.02}Y_{0.49}Sc_{0.49})_2O_3$ and $(Tm_{0.028}Y_{0.486}Sc_{0.486})_2O_3$. The detailed growth procedure is described in [28]. An Yb^{3+}(0.4 at.%):$YScO_3$ crystal was used as a seed crystal. The two as-grown crystals with different Tm^{3+}-doping levels are shown in Figs. 1(a, b). The actual composition of the grown crystals was determined to be $(Tm_{0.022}Y_{0.472}Sc_{0.506})_2O_3$ and $(Tm_{0.031}Y_{0.474}Sc_{0.495})_2O_3$ by inductively coupled plasma optical emission spectrometry (ICP-OES) at the top of the boule, from where all samples investigated here were cut. With the segregation coefficient being close to unity and the fact that we only used ~1/3 of the initial melt for the growth of the crystals, the variation of the composition throughout the crystal is estimated to be very low. The measured compositions indicate a segregation coefficient slightly higher than unity for the Tm^{3+} doping ions and lower than unity for Y^{3+} host ions. The Tm^{3+}(2.2 at.%):$YScO_3$ boule has a length of 55 mm and a diameter of 15 to 20 mm, while the Tm^{3+}(3.1 at.%):$YScO_3$ has a length of 48 mm and a diameter of 17 to 18

Optics EXPRESS

mm. The lower doped crystal grown in a static 100% argon atmosphere exhibits a brownish coloration. To quantify the corresponding absorption, we performed transmission measurements from the UV to the near-infrared spectral range using a dual-beam UV/Vis/NIR spectrometer (Perkin Elmer, Lambda 1050) set to a resolution of 1 nm. The spectra shown in Fig. 1(c) are not corrected for the Fresnel reflection of about 10% at each facet for the refractive index estimated to be ~1.9 [32]. For the as-grown crystal shown as the orange curve in Fig. 1(c), we found a broad absorption background extending from the UV range to about 1000 nm. We found this background absorption to disappear by annealing in a reducing atmosphere (forming gas with a composition of H_2:N_2 = 5:95) at 1500°C for 15 h as seen in the blue curve in Fig. 1(c). From this result, we conclude that the coloration was caused by an excess of oxygen in the growth atmosphere, however, the origin of this coloration is still unclear. The second crystal, Tm^{3+} (3.1 at.%):$YScO_3$, was grown under a continuous flow of argon to flush any residual oxygen out from the furnace. As a result, the as-grown higher doped crystal exhibits the greenish color typically found for Tm^{3+}-doped crystals and no further annealing was required for this boule.

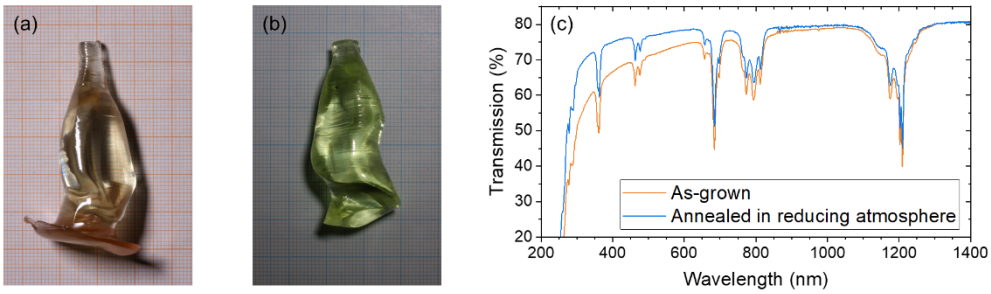

Fig. 1. Photographs of the as-grown (a) Tm^{3+} (2.2 at.%):$YScO_3$ and (b) Tm^{3+} (3.1 at.%):$YScO_3$ crystals. (c) Transmission spectra of the as-grown (orange) and annealed in reducing atmosphere (blue) Tm^{3+} (2.2 at.%):$YScO_3$ crystal shown in Fig. 1(a) in the UV to the near-infrared spectral region.

3. Spectroscopic characterization

3.1. Temperature-dependent absorption cross sections

To determine the absorption cross sections at different temperatures, we measured the temperature-dependent transmission of light emitted by a tungsten-halogen lamp through our samples. The wavelength selection of the transmitted light was performed with a monochromator (HORIBA, M1000) and a closed-cycle helium cryostat (Advanced Research Systems, DE204) was used to set the temperature of the sample. A photomultiplier tube (Hamamatsu, R5108) was used to measure the signal at wavelengths between 720 nm and 850 nm ($^3H_6 \rightarrow {}^3H_4$) and an InGaAs biased-detector (Thorlabs, DET10D2) was used for detection between 1450 nm and 2050 nm ($^3H_6 \rightarrow {}^3F_4$). The absorption band around 790 nm is interesting for two-for-one pumping by AlGaAs LDs or Ti:sapphire lasers, and the 1600 nm band can be utilized for in-band pumping by InP LDs or Er fiber lasers.

The absorption cross sections were calculated by the Beer-Lambert law using the density of Tm^{3+} ions. The ion density was derived from the doping concentration of 2.2 at.% and the lattice constant of 10.14 Å, which were determined by ICP-OES measurements and powder X-ray diffraction measurements, respectively. Figure 2 shows the resulting temperature-dependent absorption cross sections of Tm^{3+} (2.2 at.%):$YScO_3$, which are in perfect agreement with the results for higher doped sample. For both transitions ($^3H_6 \rightarrow {}^3H_4$ and $^3H_6 \rightarrow {}^3F_4$), the absorption cross section values at shorter wavelengths become pronounced at lower temperatures because of

Optics EXPRESS

the corresponding thermal depopulation of the upper Stark levels of the ground-state multiplet. This leads to a narrower absorption bandwidth at low temperatures. In the absorption band in the 800-nm range shown in Fig. 2(a), there are three prominent peaks at 300 K with peak cross sections of 2.5×10^{-21}, 2.8×10^{-21}, and 2.1×10^{-21} cm^2 at 773, 794, and 812 nm, respectively. For the absorption band in the 1600-nm range seen in Fig. 2(b), the peak cross section found at 1620 nm is 3.6×10^{-21} cm^2 at 300 K. As expected, this peak absorption wavelength is between the values of Tm^{3+}:Y_2O_3 and Tm^{3+}:Sc_2O_3 at 1634 nm and 1611 nm, respectively [25]. At 14 K, the absorption at 1620 nm increases to 7.4×10^{-21} cm^2, while the spectral bandwidth reduces from ~70 nm to ~40 nm.

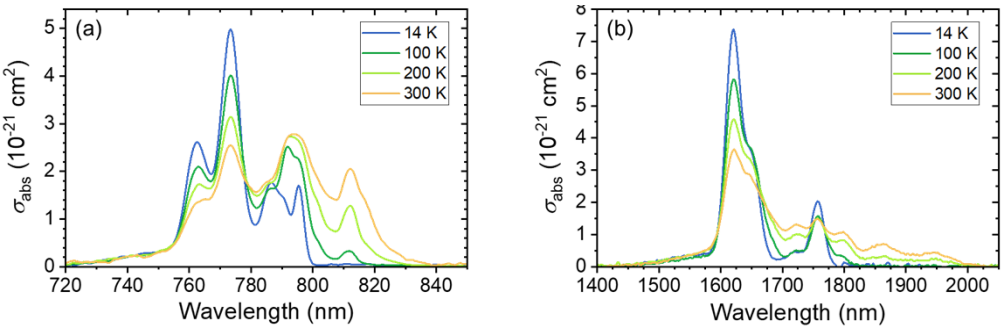

Fig. 2. Temperature-dependent absorption cross sections of the Tm^{3+} (2.2 at.%):$YScO_3$ crystal in (a) 800-nm (measured with a resolution of 1 nm) and (b) 1600-nm (measured with a resolution of 3 nm) range.

The broad absorption bands even at 14 K evidence the inhomogeneous spectral broadening caused by the disordered structure of the mixed sesquioxide crystals, as they are significantly broader than those of, *e.g.*, Tm^{3+}-doped Y_2O_3 at 40 K [33].

3.2. *Temperature-dependent fluorescence lifetime*

The temperature-dependent fluorescence lifetime of the $^3F_4$ multiplet responsible for the 2 µm laser emission was measured. To mitigate the influence of radiation trapping [34] resulting from reabsorption of emitted photons due to the partial overlap of the emission and absorption spectra of Tm^{3+}:$YScO_3$ at 2 µm [cf. Figure 2(b) and Fig. 4(a)], we prepared a Tm^{3+} (2.2 at.%):$YScO_3$ sample as thin as ≈270 µm for these measurements. The sample was excited by an optical parametric oscillator (OPO, GWU-Lasertechnik, versaScan) delivering 5-ns pulses at a 10 Hz repetition rate. We chose the excitation wavelength to be 1620 nm for in-band excitation to exclude any influence of decay and/or population from other levels on the measured decay curves. The fluorescence signal was detected by the InGaAs biased-detector and recorded by an oscilloscope. Using the cryostat, we measured the lifetimes at temperatures between 14 K and 300 K. In addition, to evaluate the residual influence of radiation trapping in the thin sample, we determined the intrinsic lifetime by applying the pinhole method [34,35] at room temperature. To this end, we prepared a second sample of more than 2.5 mm thickness and used pinholes with different diameters between 0.8 mm and 2.5 mm for these measurements. Since the setup for the pinhole method is not compatible with the cryostat, we did not use this method for the temperature-dependent lifetime measurements.

Figure 3(a) shows the typical fluorescence decay curve on a semi-logarithmic scale measured at 14 K and 300 K. The narrow peak shortly after the excitation is caused by residual excitation light, which could not be completely blocked by a long-pass filter. At 14 K we observed a single-exponential decay curve; however, the decay curve at room temperature slightly deviates from a single-exponential fit, which is attributed to the influence of activated energy migration

Optics EXPRESS

between the optically active C_2 sites and the inversion symmetric and thus weakly optically active and long living C_{3i} sites at higher temperatures [4]. The fluorescence lifetime was determined by fitting in the range between 0.5 ms to 5.0 ms after the excitation. Figure 3(b) shows the resulting temperature-dependent fluorescence lifetimes. The measured lifetime slightly decreased at lower temperatures. The fluorescence lifetime measured using the thin sample at room temperature amounts to 4.0 ms, which deviates only by ≈4% from the room-temperature fluorescence lifetime of 3.83 ms determined by the pinhole method [cf. Figure 3(c)]. While this indicates a fairly low influence of radiation trapping on all the fluorescence lifetime measurements using the thin sample, the difference between the lifetimes at 300 K and 14 K found in Fig. 3(b) is on the same order as the influence of radiation trapping. We thus conclude that the remaining variation with temperature is caused by radiation trapping and that there is no thermal quenching of the 2 µm emission at room temperature in Tm^{3+} (2.2 at.%):$YScO_3$. This is explained by the sufficiently large energy gap between the $^3F_4$ multiplet and the $^3H_6$ multiplet estimated to be ≈4750 cm^{-1} from the longest-wavelength emission peak at 14 K [cf. Figure 4(a)]: The comparably low maximum phonon energies of cubic sesquioxides (Y_2O_3: 592 cm^{-1}, Sc_2O_3: 669 cm^{-1} [36]) prohibit any significant non-radiative multi-phonon decay [37].

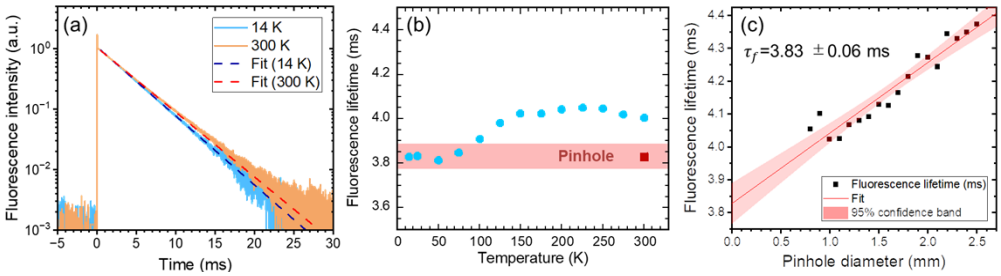

Fig. 3. (a) Fluorescence decay curves of the Tm^{3+} (2.2 at.%):$YScO_3$ at 300 K (orange) and 14 K (blue) and fit curves for 300 K (red, dashed) and 14 K (dark blue, dashed). (b) Temperature-dependent fluorescence lifetime measured using the thin-sample (blue) and determined by the pinhole method (red). The red band indicates 95% confidence band of fit for the pinhole method. (c) Fluorescence lifetime measured using pinholes with different diameters.

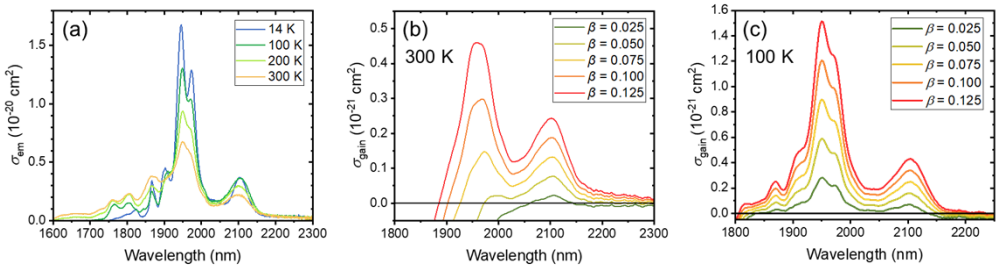

Fig. 4. (a) Temperature-dependent emission cross sections of the Tm^{3+} (2.2 at.%):$YScO_3$ crystal and gain cross sections at different inversion levels at (b) 300 K and (c) 100 K. Note the different y-axis scale between (b) and (c).

3.3. *Temperature-dependent emission and gain cross sections*

The temperature-dependent fluorescence spectra around 2000 nm corresponding to the $^3F_4 \rightarrow {}^3H_6$ transition of Tm^{3+} were measured using the monochromator, the InGaAs biased-detector, and the

Optics EXPRESS

helium cryostat described above. We measured the fluorescence in the wavelength range from 1600 to 2300 nm with a spectral resolution of 3 nm which was sufficient to resolve all spectral features. As an excitation source, we used a 780 nm LD with a spectral bandwidth of ~1 nm (FWHM). We used again the ≈270 µm thin Tm^{3+} (2.2%):$YScO_3$ sample shown to exhibit a low influence of reabsorption for fluorescence measurements. The stimulated emission cross sections σ_{em} were calculated from the fluorescence intensity spectra by the Füchtbauer-Ladenburg equation

$$\sigma_{em}(\lambda) = \frac{\lambda^5 I(\lambda)}{8\pi n^2 c \tau_{rad} \int \lambda I(\lambda) d\lambda} \tag{1}$$

where $I(\lambda)$ is the measured fluorescence intensity, while n and τ_{rad} are the refractive index and the radiative lifetime, respectively. For the radiative lifetime, we used the fluorescence lifetime value of 3.83 ms derived in section 3.2, thus assuming no temperature dependence and the absence of non-radiative decay.

Figure 4(a) shows the temperature-dependent emission cross sections. The emission peak values at 300 K are 6.8×10^{-21} cm^2 and 2.2×10^{-21} cm^2 at 1949 nm and 2099 nm, respectively. The corresponding spectral bandwidths of the peaks are 96 nm and 110 nm (FWHM). With decreasing temperature, the fluorescence peaks at shorter wavelengths decrease due to the depopulation of the upper Stark levels of the $^3F_4$ multiplet. The peak emission cross sections increase to 1.7×10^{-20} cm^2 and 3.7×10^{-21} cm^2 at 1945nm and 2103 nm, respectively, and the corresponding spectral bandwidths decrease to 54 nm and 52 nm at 14 K. Thus, also the emission peaks of Tm^{3+}:$YScO_3$ are shifted to values in-between those of Tm^{3+}:Y_2O_3 (1933 nm and 2048/2072 nm [25]) and Tm^{3+}:Sc_2O_3 (1972/1992 nm and 2115/2148 nm [4]). Compared with the pure sesquioxides, the spectra are less structured and the FWHM spectral bandwidth is broader.

We also calculated the gain cross sections σ_{gain} using the equation

$$\sigma_{gain} = \beta\sigma_{em} - (1-\beta)\sigma_{abs} \tag{2}$$

where β is the inversion level, *i.e.*, the fraction of ions in the excited state, and σ_{em} and σ_{abs} are the stimulated emission and absorption cross sections, respectively. The calculated gain cross sections at 300 K for different inversion levels are shown in Fig. 4(b). The gain spectra are broad and flat, and particularly for low inversion levels, laser operation in the water-vapor-absorption free range beyond 2000nm is possible. This gain profile should enable broad wavelength tunability and support ultrashort pulse generation. Figure 4(c) shows the calculated gain cross sections at 100 K. Compared to the room-temperature spectra, the gain at the same inversion level is increased due to the higher emission cross sections. Moreover, the gain even extends to wavelengths below 1850 nm owing to the reduced absorption in this range at lower temperatures [cf. Figure 2(b)], while the spectra are still fairly broad and smooth. These features are of high relevance for ultrafast laser amplification toward higher average and peak powers: A cryogenically cooled Tm^{3+}:Y_2O_3 ceramics amplifier reached a peak power of 45 kW at a pulse duration of 30 ns and a repetition rate of 10 Hz [22]. However, the narrow gain of Tm^{3+}:Y_2O_3 at low temperatures does not support fs-pulse durations. Cryogenically cooled Tm^{3+}:$YScO_3$ mixed sesquioxide amplifiers could overcome these limitations and enable to reach new realms of ultrafast laser pulses in the 2-µm spectral range.

4. Laser experiments

To explore the potential of Tm^{3+}:$YScO_3$ for 2-µm laser operation, we performed cw laser experiments in a short laser resonator. The experimental setup is shown in Fig. 5. We used a plane-concave (R = 50 mm) linear cavity with a length of 48 mm. As the gain media, a 6-mm thick Tm^{3+} (2.2 at%):$YScO_3$ crystal and a 4-mm thick Tm^{3+}:(3.1 at.%):$YScO_3$ crystal, both

Optics EXPRESS

remaining uncoated, were prepared. The crystals were mounted on water-cooled copper holders. We used a single-emitter C-mount LD with a maximum output power of 3 W at a wavelength around 780 nm (Roithner Lasertechnik GmbH, RLT785-4WC) as a pump source for two-for-one pumping. The LD has an emitter area of $200 \times 1\ \mu m^2$ (sagittal × tangential), consequently, the beam quality factor M^2 is about 28 and 1 for the sagittal and tangential planes, respectively. To account for this, the pump beam was shaped by a series of lenses and focused to $\sim 220 \times 60\ \mu m^2$ on the gain medium. To characterize the laser performance, five different output couplers (OCs) with transmissions of 1.0%, 3.2%, 4.0%, 5.0%, and 8.7% were used. The pump absorption varied depending on the incident pump power level because the operating wavelength of the LD changed from 775 nm to 777 nm with increasing power. Under lasing conditions, the corresponding pump absorption efficiency reduced from 63% to 57% for the 6-mm thick Tm^{3+} (2.2 at.%):$YScO_3$ sample and from 60% to 53% for the 4-mm Tm^{3+}:(3.1 at.%):$YScO_3$ sample.

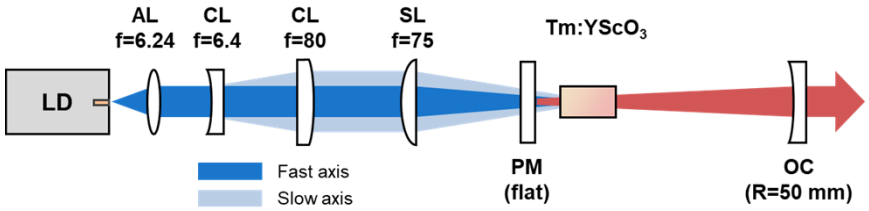

Fig. 5. Experimental setup of the cw Tm^{3+}:$YScO_3$ laser (LD: laser diode, AL: aspherical lens, CL: cylindrical lens, SL: spherical lens, PM: pump mirror, OC: output coupler).

Figure 6(a) shows the laser output power versus absorbed pump power of the Tm^{3+} (2.2 at.%):$YScO_3$ laser with different OCs. Using the lowest OC transmission of 1.0%, laser operation was obtained at a threshold absorbed pump power of only 250 mW. With increasing OC transmission, the slope efficiency increased and the best value of 35% at a maximum output power of 500 mW was obtained using the 4.0% OC. For higher OC transmissions of 5.0% and 8.7%, the slope efficiency dropped, which indicates inversion-dependent loss processes. Figure 6(b) shows the laser spectra recorded using an upconversion spectrometer (NLIR, S2050-130-hr) with a spectral resolution of $4\ cm^{-1}$. For all OCs the laser wavelengths were centered around 2100 nm [see Fig. 6(b)]. The laser spectra exhibit distinct peaks in the emission range. However, not all of the peaks were resolved owing to the limited resolution of our spectrometer. This structured emission profile would be owed to etalon effects caused by the length of the plane-parallel crystal facets and their distance to the cavity components. In addition, this broad laser emission bandwidth is typical for lasers based on inhomogeneously broadened gain materials [38,39]. The minor deviations are attributed to the particular coating of the OC mirrors used in these experiments. However, no shift of the emission wavelength to values below 2000 nm was observed, which indicates that the laser operated at moderate inversion levels below 7.5% in all experiments [cf. Figure 4(b)].

Figures 6(c, d) show the output characteristics and the free running spectra of the Tm^{3+} (3.1 at.%):$YScO_3$ laser. Using the lower transmission OCs, higher slope efficiencies were obtained compared with the Tm^{3+} (2.2 at.%):$YScO_3$ laser. This indicates a more pronounced cross relaxation owing to a closer average distance between the Tm^{3+} ions at the higher doping levels. The highest slope efficiency of 45% and the maximum output power of 422 mW were obtained using the 4.0% OC. The Stokes limit resulting from the ratio of pump and laser photon energies was only 37%, hence the 45% slope efficiency evidences a quantum efficiency higher than unity enabled by the cross-relaxation process. However, in the higher doped crystal, the laser performance strongly degraded already with the 5.0% OC and laser operation could not be obtained using the 8.7% OC. This may be explained by the closer average distance between

Optics EXPRESS

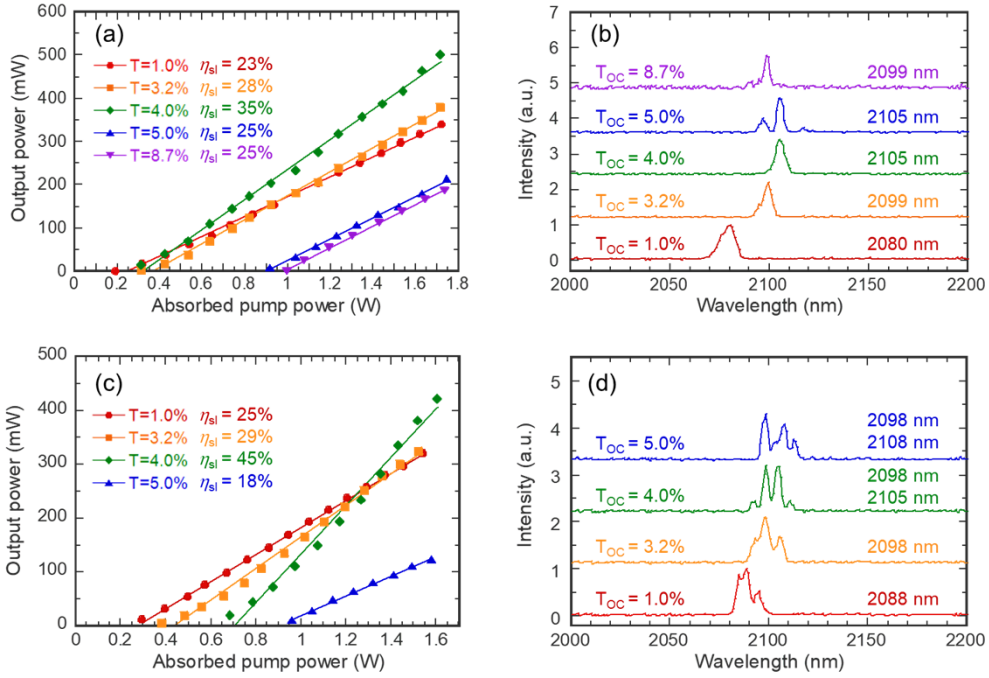

Fig. 6. Laser characteristics and free running laser spectra for different OCs of (a, b) the Tm^{3+} (2.2 at.%):$YScO_3$ laser and (c, d) the Tm^{3+} (3.1 at.%):$YScO_3$ laser.

excited ions also featuring detrimental energy transfer processes at high inversion levels. The center wavelengths were almost identical compared with the Tm^{3+} (2.2 at.%):$YScO_3$ laser for each OC. These laser efficiencies are higher than those obtained with any Tm^{3+}-doped mixed sesquioxide ceramic lasers [25,40], but they fall behind the slope efficiencies of 55% and 59% obtained with Tm:$LuScO_3$ and Tm:Lu_2O_3 crystals, respectively, which we attribute to the strong internal stress in our crystals.

5. Summary

We investigated the spectroscopic properties and the laser characteristics of the novel mixed sesquioxide gain material Tm^{3+}:$YScO_3$. For the first time, cm^3-scale laser-quality crystals were grown by the Czochralski method from iridium crucibles. In temperature-dependent spectroscopic investigations, we confirmed the absence of non-radiative relaxation processes from the upper laser level in a Tm^{3+} (2.2%)-doped $YScO_3$ crystal. The disordered nature of the mixed sesquioxide host matrix features a broadening of the absorption, which facilitates diode pumping. The corresponding broad and flat emission spectrum is promising for the generation of sub-50-fs pulses centered at wavelengths beyond 2 µm in mode-locked laser operation. In addition, due to the inhomogeneous broadening mechanism, the spectral bandwidth remains broad even at cryogenic temperatures. This indicates that Tm^{3+}:$YScO_3$ is a suitable host material for the generation of ultrashort pulses with high average and/or peak power using cryogenic amplifier technology.

Finally, we demonstrated the first diode-pumped cw Tm^{3+}:$YScO_3$ lasers. Slope efficiencies of up to 45% were achieved using a Tm^{3+} (3.1 at.%):$YScO_3$ crystal at 4.0% of OC transmission with an output power up to 0.5 W at 2.1 µm. Our laser experiments show that Tm^{3+}-doped mixed sesquioxide crystals have a huge potential for highly efficient and ultrafast lasers in the water-vapor-absorption free 2.1-µm wavelength range. The possibility to grow these materials by

Optics EXPRESS

the Czochralski method is an important step toward a future commercial availability of mixed sesquioxides.

Funding. Japan Society for the Promotion of Science (JP 21J11719).

Acknowledgments. The authors thank Dr. Andrea Dittmar for ICP-OES and Albert Kwasniewski for X-ray diffraction measurements. This work was supported by JSPS KAKENHI Grant Number JP21J11719.

Disclosures. The authors declare that there are no conflicts of interest related to this article.

Data availability. Data underlying the results presented in this paper may be obtained from the authors upon request.

References

1. Y. J. Shen, R. J. Lan, Y. C. Zhao, C. P. Qian, T. Y. Dai, and B. Q. Yao, "High-Power Diode-End-Pumped Slab Composite Tm:YLF Compact Laser," J. Russ. Laser Res. **38**(6), 559–563 (2017).
2. F. Stutzki, C. Gaida, M. Gebhardt, F. Jansen, A. Wienke, U. Zeitner, F. Fuchs, C. Jauregui, D. Wandt, D. Kracht, J. Limpert, and A. Tünnermann, "152 W average power Tm-doped fiber CPA system," Opt. Lett. **39**(16), 4671–4674 (2014).
3. K. Van Dalfsen, S. Aravazhi, C. Grivas, S. M. Garcia-Blanco, and M. Pollnau, "Thulium channel waveguide laser with 1.6 W of output power and ~80% slope efficiency," Opt. Lett. **39**(15), 4380–4383 (2014).
4. C. Kränkel, "Rare-earth-doped sesquioxides for diode-pumped high-power lasers in the 1-, 2-, and 3-µm spectral range," IEEE J. Sel. Top. Quantum Electron. **21**(1), 250–262 (2015).
5. R. Peters, C. Kränkel, S. T. Fredrich-Thornton, K. Beil, K. Petermann, G. Huber, O. H. Heckl, C. R. E. Baer, C. J. Saraceno, T. Südmeyer, and U. Keller, "Thermal analysis and efficient high power continuous-wave and mode-locked thin disk laser operation of Yb-doped sesquioxides," Appl. Phys. B **102**(3), 509–514 (2011).
6. P. A. Loiko, K. V. Yumashev, R. Schödel, M. Peltz, C. Liebald, X. Mateos, B. Deppe, and C. Kränkel, "Thermo-optic properties of Yb:Lu_2O_3 single crystals," Appl. Phys. B **120**(4), 601–607 (2015).
7. P. Koopmann, S. Lamrini, K. Scholle, M. Schafer, P. Fuhrberg, and G. Huber, "Holmium-doped Lu_2O_3, Y_2O_3, and Sc_2O_3 for lasers above 2.1 µm," Opt. Express **21**(3), 3926–3931 (2013).
8. P. Koopmann, S. Lamrini, K. Scholle, P. Fuhrberg, K. Petermann, and G. Huber, "Efficient diode-pumped laser operation of Tm:Lu_2O_3 around 2 µm," Opt. Lett. **36**(6), 948–950 (2011).
9. P. Loiko, P. Koopmann, X. Mateos, J. M. Serres, V. Jambunathan, A. Lucianetti, T. Mocek, M. Aguilo, F. Diaz, U. Griebner, V. Petrov, and C. Kränkel, "Highly efficient, compact Tm^{3+}:RE_2O_3 (RE = Y, Lu, Sc) sesquioxide lasers based on thermal guiding," IEEE J. Sel. Top. Quantum Electron. **24**(5), 1–13 (2018).
10. J. J. Sun, Y. Chen, K. Zhang, Q. K. Pan, Y. He, D. Y. Yu, and F. Chen, "Efficient continuous wave and acousto-optical Q-switched Tm:Lu_2O_3 laser pumped by the laser diode at 1.7 µm," Infrared Phys. Technol. **116**, 103771 (2021).
11. A. Schmidt, P. Koopmann, G. Hüber, P. Fuhrberg, S. Y. Choi, D. I. Yeom, F. Rotermund, V. Petrov, and U. Griebner, "175 fs Tm:Lu_2O_3 laser at 2.07 µm mode-locked using single-walled carbon nanotubes," Opt. Express **20**(5), 5313–5318 (2012).
12. A. Suzuki, C. Kränkel, and M. Tokurakawa, "High quality-factor Kerr-lens mode-locked Tm:Sc_2O_3 single crystal laser with anomalous spectral broadening," Appl. Phys. Express **13**(5), 052007 (2020).
13. A. Suzuki, C. Kränkel, and M. Tokurakawa, "Sub-6 optical-cycle Kerr-lens mode-locked Tm:Lu_2O_3 and Tm:Sc_2O_3 combined gain media laser at 2.1 µm," Opt. Express **29**(13), 19465–19471 (2021).
14. R. Peters, C. Kränkel, K. Petermann, and G. Hüber, "Crystal growth by the heat exchanger method, spectroscopic characterization and laser operation of high-purity Yb:Lu_2O_3," J. Cryst. Growth **310**(7-9), 1934–1938 (2008).
15. M. Chaika, S. Balabanov, and D. Permin, "Optical spectra and gain properties of Er^{3+}:Lu_2O_3 ceramics for eye-safe 1.5-µm lasers," Opt. Mater. **112**, 110785 (2021).
16. E. V. Ivakin, I. G. Kisialiou, and O. L. Antipov, "Laser ceramics Tm:Lu_2O_3 center dot Thermal, thermo-optical, and spectroscopic properties," Opt. Mater. **35**(3), 499–503 (2013).
17. Z. Y. Liu, G. Toci, A. Pirri, B. Patrizi, Y. G. Feng, J. B. Wei, F. Wu, Z. X. Yang, M. Vannini, and J. Li, "Fabrication, microstructures, and optical properties of Yb:Lu_2O_3 laser ceramics from co-precipitated nano-powders," J. Adv. Ceram. **9**(6), 674–682 (2020).
18. J. R. Lu, K. Takaichi, T. Uematsu, A. Shirakawa, M. Musha, K. Ueda, H. Yagi, T. Yanagitani, and A. A. Kaminskii, "Yb^{3+}: Y_2O_3 ceramics - a novel solid-state laser material," Jpn. J. Appl. Phys. **41**(Part 2, No. 12A), L1373–L1375 (2002).
19. K. Takaichi, H. Yagi, A. Shirakawa, K. Ueda, S. Hosokawa, T. Yanagitani, and A. A. Kaminskii, "Lu_2O_3:Yb^{3+} ceramics - a novel gain material for high-power solid-state lasers," Phys. Status. Solidi A **202**(1), R1–R3 (2005).
20. O. L. Antipov, A. A. Novikov, N. G. Zakharov, and A. P. Zinoviev, "Optical properties and efficient laser oscillation at 2066nm of novel Tm:Lu_2O_3 ceramics," Opt. Mater. Express **2**(2), 183–189 (2012).
21. H. T. Huang, H. Wang, and D. Y. Shen, "VBG-locked continuous-wave and passively Q-switched Tm:Y_2O_3 ceramic laser at 2.1 µm," Opt. Mater. Express **7**(9), 3147–3154 (2017).
22. F. X. Yue, V. Jambunathan, S. P. David, X. Mateos, J. Sulc, M. Smrz, and T. Mocek, "Diode-pumped master oscillator power amplifier system based on cryogenically cooled Tm:Y_2O_3 transparent ceramics," Opt. Mater. Express **11**(5), 1489–1496 (2021).

Optics EXPRESS

23. N. K. Stevenson, C. T. A. Brown, and A. A. Lagatsky, "Femtosecond Tm:Lu_2O_3 ceramic MOPA at 2080nm," presented at the Advanced Solid State Lasers 2019, ATu5A.4, Vienna Austria 2019.
24. A. A. Lagatsky, O. L. Antipov, and W. Sibbett, "Broadly tunable femtosecond Tm:Lu_2O_3 ceramic laser operating around 2070nm," Opt. Express **20**(17), 19349–19354 (2012).
25. C. Kränkel, A. Uvarova, C. Guguschev, S. Kalusniak, L. Hülshoff, H. Tanaka, and D. Klimm, "Rare-earth doped mixed sesquioxides for ultrafast lasers," Opt. Mater. Express **12**(3), 1074–1091 (2022).
26. V. V. Osipov, V. A. Shitov, R. N. Maksimov, and V. I. Solomonov, "Properties of transparent Re^{3+}: Y_2O_3 ceramics doped with tetravalent additives," Opt. Mater. **50**, 65–70 (2015).
27. Z. H. Xiao, S. J. Yu, Y. M. Li, S. C. Ruan, L. B. Kong, Q. Huang, Z. R. Huang, K. Zhou, H. B. Su, Z. J. Yao, W. X. Que, Y. Liu, T. S. Zhang, J. Wang, P. Liu, D. Y. Shen, M. Allix, J. Zhang, and D. Y. Tang, "Materials development and potential applications of transparent ceramics: A review," Mater. Sci. Eng., R **139**, 100518 (2020).
28. C. Kränkel, A. Uvarova, E. Haurat, L. Hülshoff, M. Brützam, C. Guguschev, S. Kalusniak, and D. Klimm, "Czochralski growth of mixed cubic sesquioxide crystals in the ternary system Lu_2O_3-Sc_2O_3-Y_2O_3," Acta Crystallogr., Sect. B: Struct. Sci., Cryst. Eng. Mater. **77**(4), 550–558 (2021).
29. L. Hülshoff, A. Uvarova, C. Guguschev, S. Kalusniak, H. Tanaka, D. Klimm, and C. Kränkel, "Czochralski growth and laser operation of Er- and Yb-doped mixed sesquioxide crystals," presented at the Advanced Solid State Lasers, ATh1A.2, Washington, DC United States 2021.
30. R. Moncorgé, Y. Guyot, C. Kränkel, K. Lebbou, and A. Yoshikawa, "Mid-infrared emission properties of the Tm^{3+}-doped sesquioxide crystals Y_2O_3, Lu_2O_3, Sc_2O_3 and mixed compounds $(Y,Lu,Sc)_2O_3$ around 1.5-, 2-and 2.3-μm," J. Lumin. **241**, 118537 (2022).
31. Y. G. Zhao, L. Wang, W. D. Chen, Z. B. Pan, Y. C. Wang, P. Liu, X. D. Xu, Y. Liu, D. Y. Shen, J. Zhang, M. Guina, X. Mateos, P. Loiko, Z. P. Wang, X. G. Xu, J. Xu, M. Mero, U. Griebner, and V. Petrov, "SESAM mode-locked Tm:$LuYO_3$ ceramic laser generating 54-fs pulses at 2048nm," Appl. Opt. **59**(33), 10493–10497 (2020).
32. D. E. Zelmon, J. M. Northridge, N. D. Haynes, D. Perlov, and K. Petermann, "Temperature-dependent Sellmeier equations for rare-earth sesquioxides," Appl. Opt. **52**(16), 3824–3828 (2013).
33. F. X. Yue, V. Jambunathan, S. P. David, X. Mateos, M. Aguiló, F. Diaz, J. Šulc, A. Lucianetti, and T. Mocek, "Spectroscopy and diode-pumped continuous-wave laser operation of Tm:Y_2O_3 transparent ceramic at cryogenic temperatures," Appl. Phys. B **126**(3), 44 (2020).
34. H. Kühn, S. T. Fredrich-Thornton, C. Kränkel, R. Peters, and K. Petermann, "Model for the calculation of radiation trapping and description of the pinhole method," Opt. Lett. **32**(13), 1908–1910 (2007).
35. C. Kränkel, D. Fagundes-Peters, S. T. Fredrich, J. Johannsen, M. Mond, G. Huber, M. Bernhagen, and R. Uecker, "Continuous wave laser operation of Yb^{3+}: YVO_4," Appl. Phys. B **79**(5), 543–546 (2004).
36. M. V. Abrashev, N. D. Todorov, and J. Geshev, "Raman spectra of R_2O_3 (R-rare earth) sesquioxides with C-type bixbyite crystal structure: A comparative study," J. Appl. Phys. **116**(10), 103508 (2014).
37. H. W. Moos, "Spectroscopic relaxation processes of rare earth ions in crystals," J. Lumin. **1-2**, 106–121 (1970).
38. W. Jing, P. Loiko, J. M. Serres, Y. C. Wang, E. Vilejshikova, M. Aguilo, F. Diaz, U. Griebner, H. Huang, V. Petrov, and X. Mateos, "Synthesis, spectroscopy, and efficient laser operation of "mixed" sesquioxide Tm:$(Lu, Sc)_2O_3$ transparent ceramics," Opt. Mater. Express **7**(11), 4192–4202 (2017).
39. D. Z. Li, L. C. Kong, X. D. Xu, P. Liu, G. Q. Xie, J. Zhang, and J. Xu, "Spectroscopy and mode-locking laser operation of Tm:$LuYO_3$ mixed sesquioxide ceramic," Opt. Express **27**(17), 24416–24425 (2019).
40. A. Pirri, R. N. Maksimov, J. Li, M. Vannini, and G. Toci, "Achievements and future perspectives of the trivalent thulium-ion-doped mixed-sesquioxide ceramics for laser applications," Materials **15**(6), 2084 (2022).